Enhanced pervaporation dehydration performance of ultrathin hybrid membrane by incorporating bioinspired multifunctional modifier and TiCl₄ into chitosan

Jing Zhao [a], Fei Wang [a], Fusheng Pan [a], Mingxuan Zhang [a], Xiaoyue Yang [a], Pan Li [a], Zhongyi Jiang [a,*], Peng Zhang [b], Xingzhong Cao [b], Baoyi Wang [b]

[a] Key Laboratory for Green Chemical Technology of Ministry of Education, School of Chemical Engineering and Technology, Tianjin University, Tianjin 300072, China
[b] Key Laboratory of Nuclear Analysis Techniques, Institute of High Energy Physics, Chinese Academy of Sciences, Beijing 100049, China

ARTICLE INFO

ABSTRACT

3-(3,4-Dihydroxyphenyl)propionic acid (DHPPA) was introduced as a bioinspired multifunctional modifier to mediate the *in situ* sol–gel reaction of TiCl₄ within chitosan (CS) matrix through metal–organic coordination. Ultrathin, robust chitosan–titania hybrid membranes were obtained in a facile way. The morphology, chemical and physical structures, as well as the hydrophilicity and thermal stability of hybrid membranes were extensively characterized. An ethanol/water mixture was chosen as a model system to evaluate the swelling resistance property and pervaporation dehydration performance of the hybrid membranes. The simultaneous enhancement of hydrophilicity and swelling resistance was achieved due to the presence of numerous carboxyl groups and the stable hybrid structure. The multiple interfacial interactions between polymeric and inorganic phases, as well as the steric effect of the bioinspired modifier, led to significant pervaporation performance enhancement of CS membrane. When the mass ratio of TiCl₄ to CS was 14 wt%, the hybrid membrane exhibited the optimal pervaporation performance with a permeation flux of 1403 g/(m² h) and a separation factor of 730 for 90 wt% ethanol aqueous solution at 350 K. The operation stability was also testified in long-term pervaporation separation test.

© 2013 Elsevier B.V. All rights reserved.

1. Introduction

In the past decades, polymer–inorganic hybrid membranes have been recognized as a booming research subject and have promising applications in many membrane processes such as pervaporation [1–6], gas separation [7–9] and proton exchange membrane [10–12]. Presently, there are two commonly used approaches to acquire hybrid polymer–inorganic membranes according to the incorporation way of inorganic moiety into polymer bulk: physical blending and *in situ* sol–gel reaction [13,14]. Compared to physical blending, the *in situ* sol–gel reaction can form covalent bonds between the polymeric phase and inorganic phase during the hydrolysis and polycondensation process of inorganic precursor [4,15–18]. Therefore, enhanced swelling resistance can be achieved [4,15,19–21]. Moreover, the *in situ* formation of inorganic particles favors their homogeneous dispersion within polymer matrix, and inhibits the aggregation of particles and the formation of nonselective voids [4,22,23].

Conceivably, too fast of a sol–gel reaction rate will generate inorganic particles with poor uniformity and controllability during membrane fabrication [3,24,25]. In severe cases, phase separation within membranes or particle precipitation in membrane casting solution may occur [22]. To solve this problem, several strategies have been developed to manipulate the sol–gel reaction rate. One common method is utilizing chelating agents to occupy part of the reaction sites on inorganic precursors, realizing the controllable formation of inorganic particles with small size by decreasing reaction activity and producing steric hindrance [3,23,26]. For instance, Yang et al. [3] and Chen et al. [23] employed acetyl acetone to chelate with Ti atom, which slowed down the hydrolysis and polycondensation reaction of tetrabutyl titanate in polymeric matrix, achieving the homogeneous dispersion of titania nanoparticles. In these cases, the chelator just played a single role as an inhibitor of sol–gel reaction. The incorporation of a multifunctional chelator into the *in situ* sol–gel reaction would be more desirable.

The metal–organic coordination existing in the bioadhesion process has triggered considerable research interest since the discovery of metal-fortified adhesion phenomenon in marine organisms [27–30]. It is revealed that the catechol groups of 3, 4-dihydroxy-ʟ-phenylalanine (DOPA) in adhesive proteins play key

---

roles in adhesion and can chelate with almost all the transition metals [27,28,31,32]. Inspired by this phenomenon, various natural or synthesized catecholic molecules with different functional groups have been extensively employed to modify metal surfaces in a facile and efficient way [33–35]. One or more types of functional groups (such as carboxyl group, amino group, and sulfonic group) could be introduced into polymer–inorganic hybrid materials by employing specific catecholic molecules in the *in situ* sol–gel process.

In this study, a multifunctional modifier (3-(3,4-dihydroxyphenyl)propionic acid) (DHPPA) was incorporated to mediate the preparation process of hybrid membranes using chitosan (CS) as the membrane bulk matrix, and TiCl$_4$ as inorganic precursor. On the one hand, the strong chelating ability between Ti atoms and catechol groups on DHPPA inhibited the sol–gel reaction of TiCl$_4$, and then manipulated the hybrid membrane structure. As a result, robust and ultrathin membranes were fabricated in a facile approach. On the other hand, the carboxyl groups on DHPPA could improve the membrane hydrophilicity and form hydrogen bond and electrostatic attraction with amino and hydroxyl groups on CS. The morphology, chemical and physical structures, as well as the hydrophilicity and thermal stability of the hybrid membranes were characterized. The pervaporation performance and swelling resistance of the hybrid membranes were evaluated using ethanol/water mixture as a model system.

2. Experimental

2.1. Materials

Chitosan with a viscosity–average molecular weight of 450,000 (90.2% N-deacetylation degree) was obtained from Jinan Haidebei Marine Bioengineering Co. Ltd. (Jinan, China). The flat-sheet polyacrylonitrile (PAN) ultrafiltration membrane with a molecular weight cut-off of 100,000 was received from Shanghai MegaVision Membrane Engineering & Technology Co. Ltd. (Shanghai, China). 3-(3,4-Dihydroxyphenyl)propionic acid (98 wt%) was supplied by Alfa Aesar. Titanium tetrachloride (≥99 wt%) was obtained from Tianjin Suzhuang Chemical Reagent Factory (Tianjin, China). Acetic acid (≥99.5 wt%), glutaraldehyde (GA) (50 wt%) and hydrochloric acid (36–38 wt%) were purchased from Tianjin Kewei Ltd. (Tianjin, China). Absolute ethanol (≥99.7 wt%) was received from Tianjin Guangfu Fine Chemical Research Institute (Tianjin, China). All the reagents were of analytical grade and used without further purification. Deionized water was used throughout the experiments.

2.2. Membrane preparation

The hybrid membranes were prepared *via* spin-coating. First, the PAN ultrafiltration membranes (10 cm × 10 cm) were soaked in deionized water for 2 days to remove glycerin from the surfaces, and then fully dried. Afterwards, 2 wt% CS solution was prepared by dissolving CS in 2 wt% acetic acid solution at 80 °C with stirring for 2 h. Meanwhile, TiCl$_4$ was added into a 2:1 (v:v) water–ethanol mixture at room temperature and stirred for 2 h, and then DHPPA was added into TiCl$_4$ solution (the molar ratio of TiCl$_4$ to DHPPA was 4:1). After stirring for 1 h, a certain amount of the TiCl$_4$–DHPPA reaction mixture solution was added into CS solution and stirred at 60 °C for 2 h to accelerate the polycondensation of TiCl$_4$. Finally, GA was added for further cross-linking (the molar ratio of CS monomer unit to GA was 60). After filtrated and kept still for several minutes to remove air bubbles in the solution, the membrane casting solution was spin-coated on PAN ultrafiltration membranes to obtain composite membranes. The resulting

membranes were designated as CS–Ti(*X*)–DHPPA/PAN, where *X* represented the mass ratio of TiCl$_4$ to CS (wt%), varying from 0 to 28. For comparison, the membrane without DHPPA was fabricated and the mass ratio of TiCl$_4$ to CS was chosen at 14 wt%, designated as CS–Ti(14)/PAN. Moreover, the corresponding homogeneous membranes were simultaneously prepared by casting the solutions on glass plates for characterization and swelling study, designated as CS–Ti(*X*)–DHPPA or CS–Ti(*X*).

2.3. Membrane characterization

Fourier transform infrared spectra (FT-IR) of the TiCl$_4$ solutions and membranes in the range of 4000–500 cm^{-1} were recorded on a BRUKER Vertex 70 FT-IR spectrometer equipped with a horizontal attenuated transmission accessory for solutions and a horizontal attenuated total reflectance accessory for membranes. The microstructure of membrane matrix and topography of membrane surfaces were observed by field emission scanning electron microscope (FESEM) (Nanosem 430) and atomic force microscope (AFM) (CSPM 5000), respectively. The thickness of the active layer was obtained through the cross-section image of composite membrane, on which ten different locations were measured and averaged to acquire the final result. The titanium element distribution was recorded by energy-dispersive X-ray spectroscopy (EDX) equipped on FESEM. The crystalline structure of membrane was investigated using an X-ray diffraction (XRD) (Rigaku D/max 2500 v/pc) in the range of 3–55° at the scan rate of 5° min^{-1}. The static contact angle of the membrane was measured at room temperature by a contact angle goniometer (JC2000C Contact Angle Meter). To understand the thermal properties of the membranes, thermogravimetric analysis (NETZSCH TG 209 F3) was used over the range 40–800 °C using a heating rate of 10 °C min^{-1} under nitrogen flow. Measurements of positron annihilation spectroscopy (PAS) using one high-purity Ge detector were taken in a ^{22}Na slow positron beamline at room temperature to probe the free volume property of membranes. The energy of the positrons could be continuously varied in the range of 0.18–20 keV.

2.4. Swelling studies

The homogeneous membranes with different TiCl$_4$ contents were weighed and measured after they were dried in a vacuum oven and then immersed into 90 wt% ethanol aqueous solution at 350 K for 48 h to achieve sorption equilibrium. Subsequently, the membrane surfaces were wiped with tissue paper then weighed and measured quickly to obtain the mass and area of the swollen membranes. All the experiments were repeated three times. The mass swelling degree (MSD, %) and area swelling degree (ASD, %) could be calculated by

$$MSD = \frac{W_S - W_D}{W_D} \times 100 \tag{1}$$

$$ASD = \frac{A_S - A_D}{A_D} \times 100 \tag{2}$$

where W_S and W_D are the mass of the swollen and dry membranes (g), A_S and A_D are the area of the swollen and dry membranes (m^2), respectively.

2.5. Pervaporation experiment

Pervaporation experiments were performed on the P-28 membrane module (CM-Celfa AG Company, Switzerland). During the experiments, the effective membrane area in contact with feed was 25.6 cm^2, and the permeate side of the membrane was kept at

low pressure (below 0.3 kPa) using a vacuum pump, while the flow rate of feed was controlled at 60 L/h. When the steady state reached (about 1 h after start-up), the permeate was collected in the cold trap immersed in liquid nitrogen and taken out at fixed intervals. The compositions of feed and permeate solutions were analyzed by gas chromatography (Agilent4890, USA) equipped with a thermal conductivity detector (TCD) and a column packed with GDX103 (Tianjin Chemical Reagent Co., China). The separation performance of hybrid membranes was evaluated by permeation flux (J, g/(m² h)), separation factor (α) and pervaporation separation index (PSI) calculated via the following equations:

$$J = \frac{Q}{A\,t} \qquad (3)$$

$$\alpha = \frac{P_W/P_E}{F_W/F_E} \qquad (4)$$

$$\text{PSI} = J(\alpha - 1) \qquad (5)$$

where Q is the mass of permeate (g) collected during a time interval of t (h), A is the effective membrane area in contact with the feed (m²). P and F represent the mass fractions of water (with the subscript W) or ethanol (with the subscript E) in the permeate and feed solutions, respectively.

In addition, the permeance of individual components ($(P/l)_i$, GPU) (1 GPU = 7.501×10^{-12} m³(STP)/m² s pa) and selectivity (β) were calculated by the following equations:

$$(P/l)_i = \frac{J_i}{p_{i0} - p_{il}} = \frac{J_i}{\gamma_{i0} x_{i0} p_{i0}^{sat} - p_{il}} \qquad (6)$$

$$\beta = \frac{(P/l)_W}{(P/l)_E} \qquad (7)$$

where J_i is the permeation flux of component i (g/(m² h)), l is the thickness of membrane (m), p_{i0}, p_{il} are the partial pressures of component i in the feed side and permeate side (Pa), and p_{il} can be calculated approximately as 0 for the high vacuum degree in the permeate side. γ_{i0} is the activity coefficient of component i in the feed liquid, x_{i0} is the mole fraction of the component i in the feed liquid, p_{i0}^{sat} is the saturated vapor pressure of pure component i (Pa). The permeation flux of water and ethanol should be transformed into the volumes under standard temperature and pressure (STP): 1 kg of water vapor at STP = 1.245 m³ (STP), 1 kg of ethanol vapor at STP = 0.487 m³ (STP) [36]. It should be mentioned that all the experiments were performed using 90 wt% ethanol aqueous solution, and repeated for three times to guarantee the validity of experimental data.

3. Results and discussion

3.1. Membrane characterization

3.1.1. Formation of hybrid membranes

The chemical reactions involved in the fabrication of hybrid membranes are: hydrolysis, chelation, polycondensation and intermolecular dehydration. First, the hydrolysis of TiCl₄ occurred in the water–ethanol mixture, producing a number of hydroxyl groups. Then, part of the Ti atoms chelated with the catechol groups on DHPPA, consuming a certain proportion of hydroxyl groups. The pH value of TiCl₄ solution was around 1.0, which was suitable for the formation of chelate complex [37]. In the last step, polycondensation of hydroxyl groups linked with Ti atoms and their dehydration reaction with hydroxyl groups on CS formed the cross-linked hybrid structure (Fig. 1).

During the membrane fabrication process, the colorless solution of TiCl₄ in the mixture of water and ethanol turned red upon
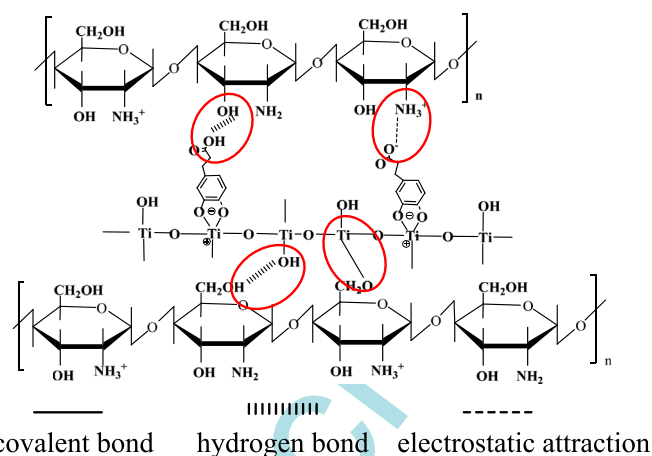

covalent bond　　　hydrogen bond　　electrostatic attraction

Fig. 1. Schematic representation of the possible chemical structure and interactions in hybrid membranes.

the addition of DHPPA. This phenomenon did not occur in the absence of TiCl₄, indirectly verifying the existence of the interaction between TiCl₄ and DHPPA. For comparison, TiCl₄ solution with or without DHPPA was heated to 60 °C and stirred for 2 h. It was observed that no precipitates appeared in the solution with DHPPA, while white precipitates emerged rapidly in the solution without DHPPA. These results indicated that DHPPA served as an inhibitor for the hydrolysis and polycondensation reaction of TiCl₄.

3.1.2. Morphology of hybrid membranes

The cross-section morphology of CS–Ti(14)–DHPPA/PAN composite membrane was characterized by FESEM and shown in Fig. 2 (a). It was revealed that the ultrathin active layer of hybrid membrane was tightly coated on the PAN membrane with a thickness around 250 nm. The EDX Ti-mapping of the cross-section of CS–Ti(14)–DHPPA membrane in Fig. 2(b) showed that titanium element was distributed uniformly in the CS matrix, indicating the homogeneous hybrid structure.

The surface morphologies of CS control membrane and hybrid membranes characterized by AFM are shown in Fig. 3. The membrane surface roughness S_q was measured via a program in the AFM image processing toolbox. It was clear that the surface roughness increased with the incorporation of Ti–DHPPA complex into CS matrix (Fig. 3(a–c)). Abundant gibbosities were distributed homogeneously on membrane surfaces, and became more evident with the increase of TiCl₄ content. The results indicated that inorganic particles were formed uniformly in CS matrix, and became larger with the TiCl₄ content increasing [19]. Comparing Fig. 3(b) with Fig. 3(d), it could be found that the membranes with or without DHPPA had similar S_q value. Nevertheless, some big protuberances with the height of 60–80 nm emerged on the surface of CS–Ti(14)/PAN, implying that the inorganic particles with heterogeneous distribution and larger size were generated in the absence of DHPPA.

3.1.3. Chemical and physical structure of hybrid membranes

The FT-IR spectra of TiCl₄ solution with or without DHPPA were compared to analyze the interactions between TiCl₄ and DHPPA as shown in Fig. 4(a). In the presence of DHPPA, the characteristic peak of Ti–O–C at around 1120 cm⁻¹ emerged, implying the chelation between Ti atoms and catechol groups on DHPPA. Meanwhile, a series of adsorption peaks appeared in the range of 1700–1200 cm⁻¹, which were assigned to the groups on DHPPA. Fig. 4(b) shows the spectra of CS control membrane and hybrid membranes. The characteristic peak at 3370 cm⁻¹ in CS membrane could be ascribed to the stretching vibration of –OH
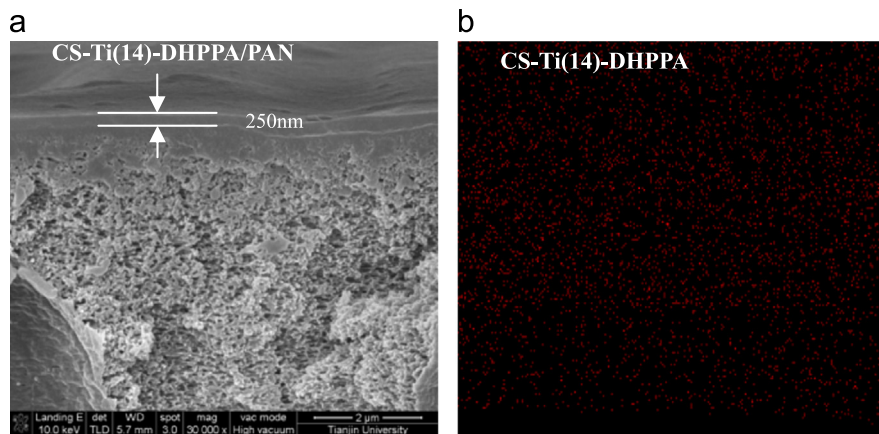
Fig. 2. (a) Cross-section morphology of CS–Ti(14)–DHPPA/PAN membrane and (b) EDX of CS–Ti(14)–DHPPA membrane (Ti distribution).
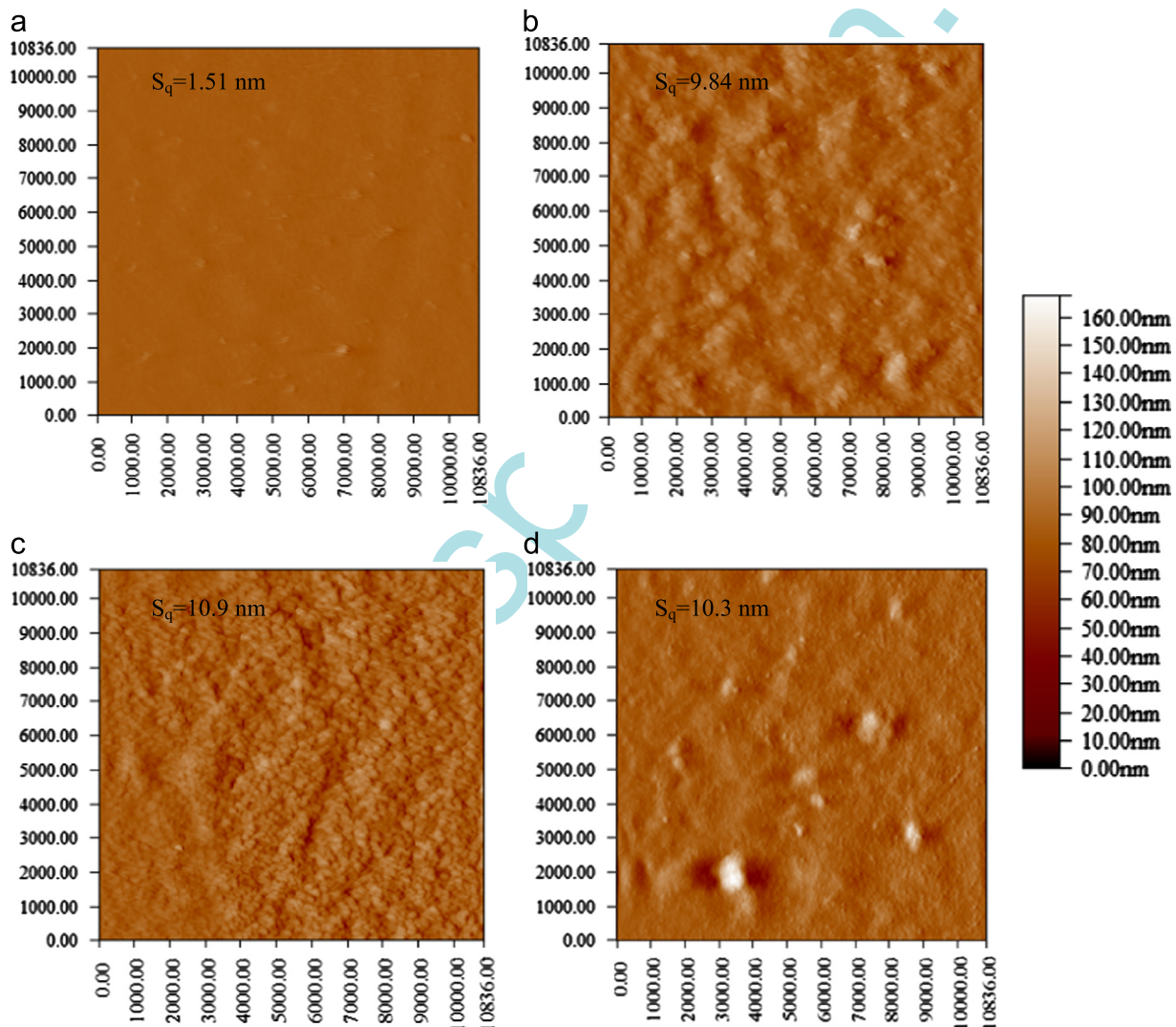

Fig. 3. AFM surface topographic images of membranes: (a) CS/PAN, (b) CS–Ti(14)–DHPPA/PAN, (c) CS–Ti(28)–DHPPA/PAN, and (d) CS–Ti(14)/PAN.

and –NH$_2$, while the peaks at 1650 cm^{-1} and 1580 cm^{-1} corresponded to the stretching vibration of C=O, and bending vibration of N–H. After the incorporation of Ti–DHPPA complex into CS matrix, all the above peaks shifted towards the lower wave number region due to the interactions between the polymeric phase and inorganic phase. Meanwhile, the peak intensity at

around 700 cm^{-1} increased apparently, which may be attributed to the formation of Ti–O–Ti [21]. Compared with other hybrid membranes, CS–Ti(14) membrane exhibited more prominent variations due to the more residual Ti–OH to interact with CS. Finally, it should be noted that the characteristic peaks of DHPPA and Ti–O–C in membranes were overlapped by the peaks from CS.
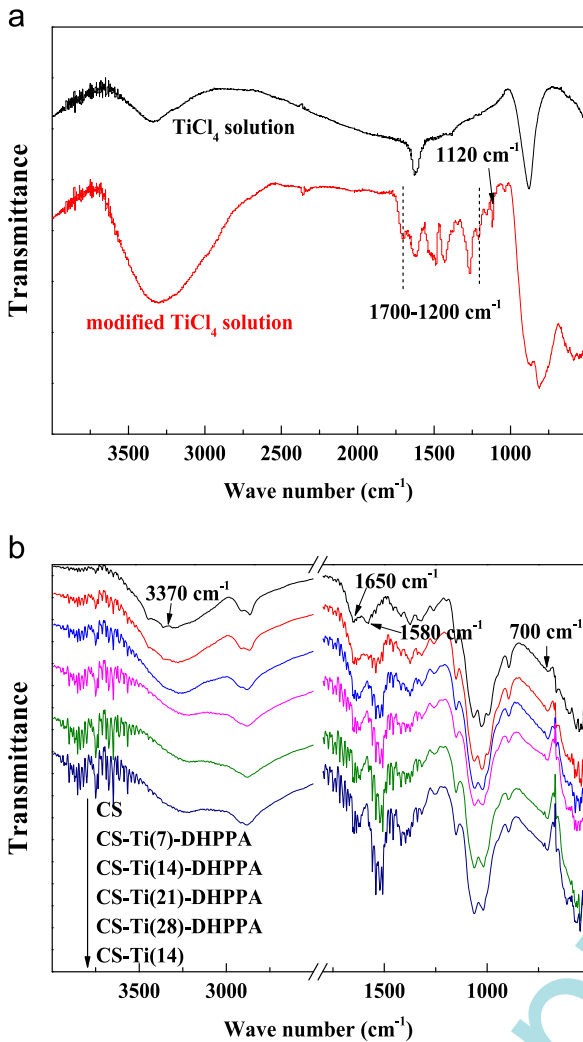
groups on CS chains. After incorporating Ti–DHPPA complex into CS matrix, no new peaks appeared, verifying that Ti existed in hybrid membranes in an amorphous form. It could be also found that the characteristic peaks of CS at $2\theta = 8.9°$ disappeared, while other peaks were broadened and showed a reduced intensity with the $TiCl_4$ content increasing. The decrease of CS crystallinity may arise from the multiple interactions of CS with the Ti–DHPPA complex, which interfered the ordered packing of polymer chains.

It should be pointed out that the characterization results of CS–Ti(28)–DHPPA membrane were not presented here because it was not able to acquire an integral, defect-free homogeneous membrane at such high $TiCl_4$ content. This can be explained by the preferential polycondensation of inorganic precursor at high $TiCl_4$ content instead of cross-linking with CS. As a result, cohesive inorganic domains were formed and then broke up the hydrogen bonds between CS chains [15,37].

To investigate the effect of Ti–DHPPA complex on the free volume property of CS membrane, the positron annihilation Doppler broadening energy spectra were obtained and described with S parameter. The S parameter is defined as the ratio of the central part of the annihilation spectrum to the total spectrum, which decreases if the size or concentration of the positron trapping cavities decreases, indicating the increased membrane compactness. Fig. 6 shows the $S–E$ curves for the CS control membrane and hybrid membranes. It should be noted that the S values with positron incident energy lower than 4 keV represented the free volume property of active layer. Comparing the $S–E$ curves of CS control membrane and CS–Ti(X)–DHPPA/PAN membranes, it was revealed that the membrane compactness first increased and then decreased with the $TiCl_4$ content increasing. After incorporating Ti–DHPPA complex into CS matrix, a cross-linked hybrid structure was formed via multiple interactions between polymeric and inorganic phases, increasing the membrane compactness. At higher $TiCl_4$ content, the cross-linking reaction of inorganic precursor with CS weakened for the increasing polycondensation propensity [15,38], leading to a loose membrane structure. Comparing the $S–E$ curves of CS–Ti(14)–DHPPA/PAN and CS–Ti(14)/PAN membranes, it could be deduced that the CS–Ti(14)–DHPPA/PAN membrane had a relatively loose structure. The reason was that the incorporated modifier DHPPA effectively deterred the densification of CS polymer chains through steric hindrance effect and suppressing the cross-linking reaction between CS and inorganic precursor.

Fig. 4. FT-IR spectra of (a) $TiCl_4$ solutions with or without modifier and (b) CS control membrane and hybrid membranes.
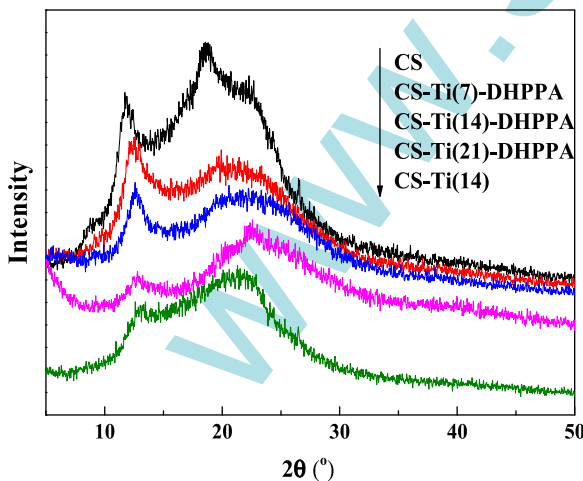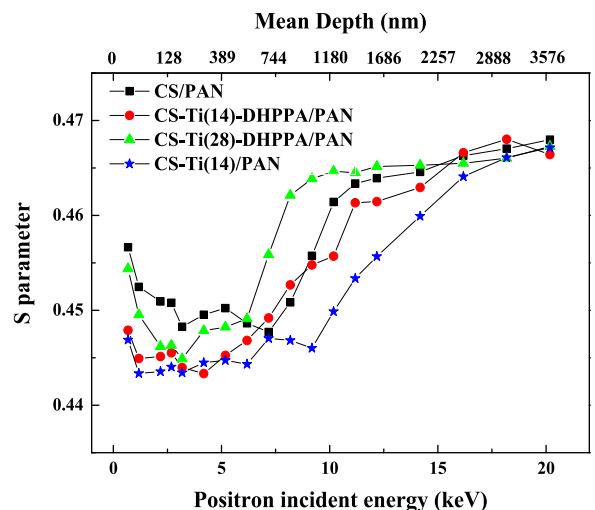

Fig. 5. XRD patterns of CS control membrane, and CS–Ti(14)–DHPPA, CS–Ti(28)–DHPPA, CS–Ti(14) hybrid membranes.

The XRD patterns of CS control membrane and hybrid membranes are shown in Fig. 5. CS is a kind of semi-crystalline polymer exhibiting characteristic peaks at around 8.9°, 11.8°, 18.7° and 22.6° for the hydrogen bonds among plenty of hydroxyl and amino

Fig. 6. S parameter as a function of the positron incident energy for CS/PAN control membrane, and CS–Ti(14)–DHPPA/PAN, CS–Ti(28)–DHPPA/PAN, CS–Ti(14)/PAN hybrid membranes.

3.1.4. Hydrophilicity and stability of hybrid membranes

The hydrophilicity of the membrane surface was evaluated by measuring the static contact angle with water as probe liquid. It is shown in Fig. 7 that the contact angles exhibited a successive decreasing tendency with the increase of $TiCl_4$ content, implying the increased hydrophilicity of membrane surface. This was caused by the carboxyl groups on DHPPA and the residual hydroxyl groups produced by the hydrolysis of $TiCl_4$, which compensated the consumed hydroxyl groups on CS in the intermolecular dehydration process. Compared with CS–Ti(14)–DHPPA/PAN membrane, the CS–Ti(14)/PAN membrane was endowed with a lower hydrophilicity, because no carboxyl group was introduced, and meanwhile a larger proportion of hydroxyl groups were consumed, leading to the decreased number of polar groups in membrane.

The thermal stability of CS control membrane and hybrid membranes were evaluated by TGA (Fig. 8) in the range of 40–800 °C. The entire thermal degradation process included three major weight loss stages: the first stage for the evaporation of residual water in the membrane (40–150 °C), the second stage for the deacetylation and depolymerization of CS (200–350 °C), and the third stage for the residual decomposition of CS (350–800 °C). Among them, the degradation behavior of CS in the second stage was the foremost to evaluate the thermal stability of the membrane. From the curves in Fig. 8, it could be deduced that the initial degradation temperatures for CS control membrane and CS–Ti
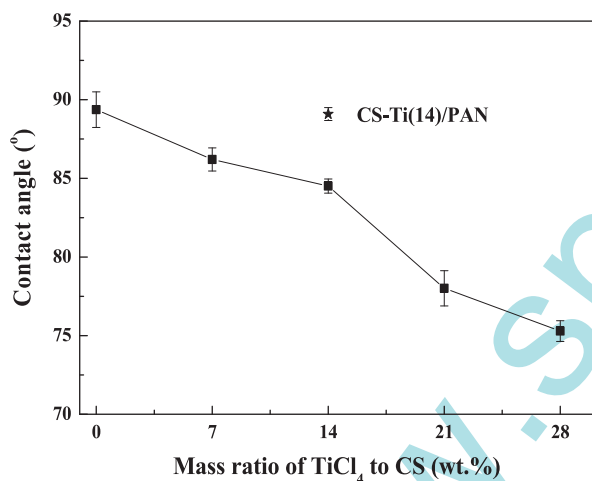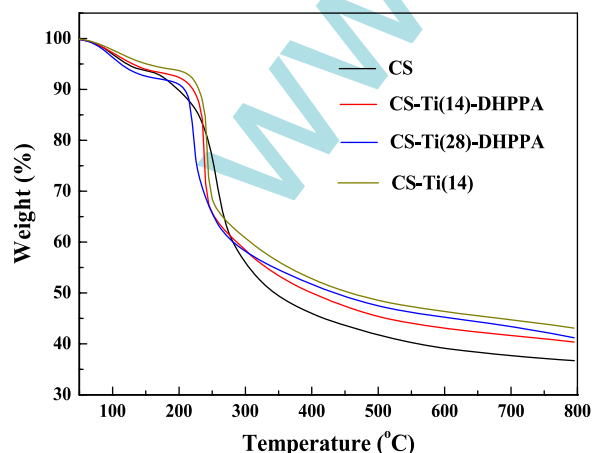
(14)–DHPPA, CS–Ti(28)–DHPPA hybrid membranes were 198.2 °C, 220.7 °C, and 207.6 °C, respectively. After incorporating Ti–DHPPA complex into CS matrix, the multiple interactions including covalent bonds, hydrogen bonds and electrostatic attractions between polymeric and inorganic phases inhibited the mobility of CS polymer chains, exhibiting an increased thermal stability. With the continuous increase of $TiCl_4$ content, the decrease of covalent bonds led to a weaker inhibition for the mobility of CS polymer chains, and a decreased thermal stability compared with CS–Ti(14)–DHPPA membrane. Comparing the TGA curves of CS–Ti(14)–DHPPA and CS–Ti(14) membranes, it could be found that the CS–Ti(14)–DHPPA membrane showed a relatively low initial degradation temperature. This phenomenon was caused by the reduced hydroxyl groups linking with Ti atoms resulting from the Ti–catechol chelation.

Swelling is a common phenomenon for hydrophilic membranes in aqueous solution, and has critical impacts on the structure and performance of membranes. Mass and area swelling degrees of membranes after immersed in 90 wt% ethanol aqueous solution at 350 K for 48 h were evaluated to reflect the membrane structure stability as shown in Fig. 9 [39]. It was noted that both the mass and area swelling degrees decreased at first with the addition of Ti–DHPPA complex, and then increased at higher $TiCl_4$ contents, while the CS–Ti(14) membrane exhibited the minimum mass and area swelling degree. The variation tendency could be primarily ascribed to the varied strength of interactions between polymeric and inorganic phases and the consequent polymer chain mobility as described in TGA characterization. Together with the static contact angle data, it could be concluded that the enhanced hydrophilicity and swelling resistance were obtained simultaneously for the hybrid membranes at appropriate $TiCl_4$ content.

3.2. Pervaporation experiment

3.2.1. Effect of $TiCl_4$ content and modifier

In order to explore the effect of incorporating Ti–DHPPA complex on the pervaporation performance of membrane, CS control membrane and hybrid membranes with different mass ratios of $TiCl_4$ to CS were fabricated and evaluated with 90 wt% ethanol aqueous solution at 350 K as shown in Fig. 10. It is revealed in Fig. 10(a) that the permeation flux decreased slightly at the beginning and then increased, while the separation factor increased significantly at first and then decreased with the mass ratio of $TiCl_4$ to CS varying from 0 wt% to 28 wt%. When the $TiCl_4$ content was lower than 14 wt%, a favorable membrane

Fig. 7. The static water contact angles on the membrane surfaces.

Fig. 8. TGA curves of CS control membrane and CS–Ti(14)–DHPPA, CS–Ti(28)–DHPPA, CS–Ti(14) hybrid membranes.
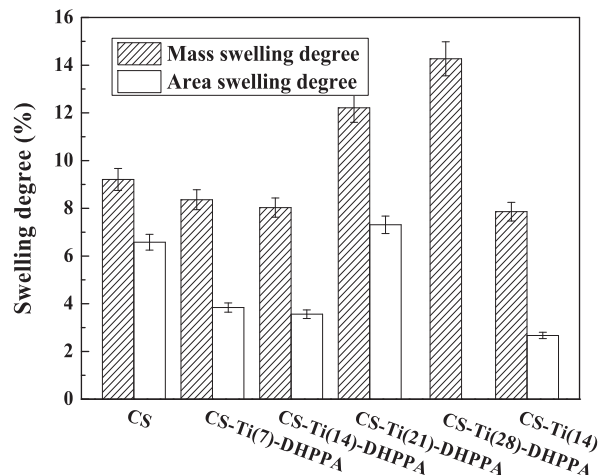

Fig. 9. Mass and area swelling degrees of CS control membrane and hybrid membranes.
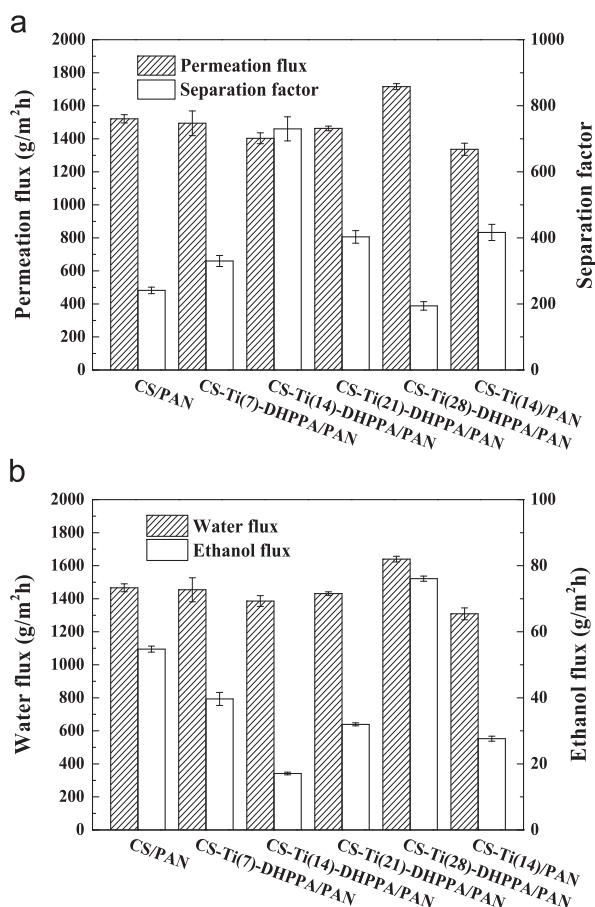
Fig. 10. The pervaporation performance of CS control membrane and hybrid membranes.

Fig. 11. (a) Effect of operation temperature on the pervaporation performance of CS–Ti(14)–DHPPA/PAN membrane, (b) Arrhenius plots of permeation flux for separating ethanol/water mixture by CS–Ti(14)–DHPPA/PAN membrane.

compactness and swelling resistance was obtained through the modified sol–gel process and steric hindrance effect of DHPPA. In addition, the hydrophilicity of hybrid membranes increased, favoring the preferential sorption of water molecules on membrane surfaces. The combination of favorable membrane compactness, increased swelling resistance and hydrophilicity resulted in the remarkable enhancement of separation factor and the slight variation of permeation flux. It is shown in Fig. 10(b) that the ethanol flux exhibited a more significant reduction than water flux, implying the improved ethanol resistance of CS membrane after incorporating Ti–DHPPA complex. When the mass ratio of $TiCl_4$ to CS was higher than 14 wt%, the loosened membrane structure and decreased swelling resistance rendered lower diffusion resistance for permeate molecules, leading to the increased permeability and decreased selectivity. Accordingly, both water flux and ethanol flux increased rapidly.

In order to evaluate the function of DHPPA in improving the separation performance of the hybrid membranes, the membrane prepared in the absence of DHPPA with the $TiCl_4$ content of 14 wt% (CS–Ti(14)/PAN membrane) was tested in pervaporation experiment with 90 wt% ethanol aqueous solution at 350 K. Fig. 10(a) shows that the CS–Ti(14)–DHPPA/PAN membrane had higher permeation flux and separation factor than CS–Ti(14)/PAN membrane for the favorable compactness and increased hydrophilicity.

3.2.2. Effect of operation temperature

Pervaporation experiments under different temperatures ranging from 303 to 350 K were carried out employing CS–Ti(14)–DHPPA/PAN membrane. It is shown in Fig. 11(a) that both
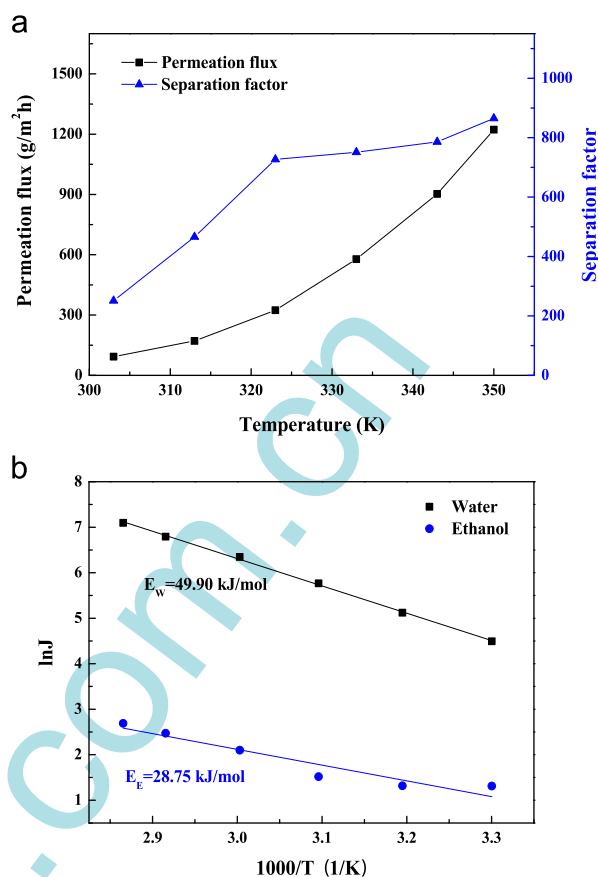
Table 1
Permeance and selectivity of CS–Ti(14)–DHPPA/PAN membrane under different temperatures.

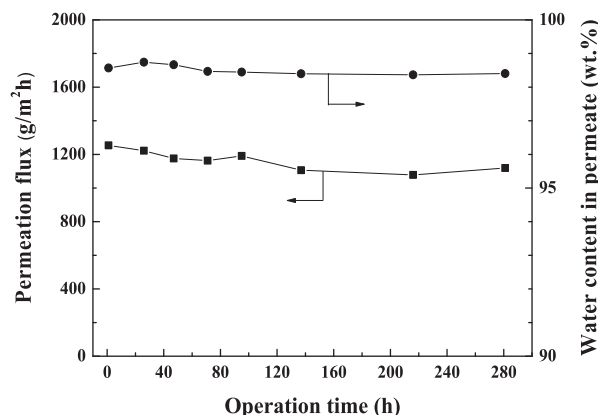| Temperature (K)	$(P/l)_W$ (GPU)	$(P/l)_E$ (GPU)	Selectivity
303	2149	7.94	270
313	2305	4.68	493
323	2606	3.48	749
333	2930	3.89	753
343	2879	3.69	780
350	3041	3.58	849

Fig. 12. The long-time pervaporation performance of the CS–Ti(14)–DHPPA/PAN hybrid membrane.

Table 2
Comparison of pervaporation performance of chitosan-based hybrid membranes for dehydration of ethanol.

Hybrid membrane	Temperature (K)	Water content in feed (wt%)	Thickness of active layer (μm)	Pervaporation performance			Reference
				Permeation flux (g/m^2 h)	Separation factor	PSI (10^5)	
CS–Ti–DHPPA/PAN	350	10	0.25	1403	730	10.23	This work
CS–APTEOS	323	15	18	900	600	5.39	[40]
CS–TEOS	353	10	45	284	460	1.30	[41]
CS–TBT	353	10	–	340	196	0.66	[3]
CS–HZSM5	353	10	25	231	153	0.35	[42]
CS–MWNT/PAN	333	10	3.27	340	573	1.94	[43]
CS–HY zeolite	298	10	–	353	102	0.36	[44]
CS–POSS1	303	10	30–40	30	373	0.11	[45]
CS–POSS2	303	10	30–40	28	306	0.09	[45]
CS–S-silica	343	10	30	410	1102	4.51	[46]
CS–TiO$_2$	353	10	–	287	207	0.59	[3]
CS–S–HZSM5	353	10	–	279	274	0.76	[47]
CS–H$_{14}$P$_5$	303	10	40	110	35,991	39.59	[2]

APTEOS: 3-aminopropyl-triethoxysilane; TEOS: tetraethoxysilane; TBT: tetrabutyl titanate; MWNT: multiwalled carbon nanotubes; POSS: polyhedral oligosilsesquioxane; S-silica: silica functionalized with sulfonic acid groups; H$_{14}$P$_5$: H$_{14}$[NaP$_5$W$_{30}$O$_{110}$].

permeation flux and separation factor kept increasing with the increase of operation temperature. The impacts of operation temperature on pervaporation process included three aspects: the mobility of permeate molecules, the membrane structure, and the interactions between permeate molecules and membrane. In general, permeation flux would increase at higher temperature for the higher mobility of permeate molecules, loosened membrane structure, and increased driving force. In contrast, the separation factor may exhibit a quite different trend. In this study, the apparent activation energy for the permeation of water and ethanol in the range of 303–350 K were calculated from the slope of the best-fit lines shown in Fig. 11(b) according to the following equation:

$$J_i = A_i \exp\left(-\frac{E_i}{RT}\right) \tag{8}$$

where J_i, A_i, E_i, R and T represent the permeation flux, pre-exponential factor, apparent activation energy, gas constant and feed temperature, respectively. The higher apparent activation energy of water (49.90 kJ/mol) compared with ethanol (28.75 kJ/mol) implied the higher temperature sensitivity of water permeation over ethanol permeation, which consequently caused the increase of separation factor. In order to analyze the impacts of temperature on pervaporation performance, the permeance (driving force-normalized form of permeation flux) and selectivity are calculated and listed in Table 1. With the increase of temperature, the water permeance kept increasing, while ethanol permeance decreased notably at first and then fluctuated slightly. It could be deduced that the increase of water flux was attributed to the combined effect of increased driving force and loosened membrane structure. With regard to ethanol, the loosened membrane structure had minor impact on the increase of the permeation flux. The continuous increase of selectivity indicated the enhanced ethanol resistance with the increase of operation temperature.

3.2.3. Long-term operation stability

The long-term operation stability is a vital factor for the industrial application of membrane. Fig. 12 shows the long-term pervaporation performance test of the CS–Ti(14)–DHPPA/PAN hybrid membrane up to 280 h for 90 wt% ethanol aqueous solution at 350 K. During the entire test, the permeation flux and water content in permeate remained almost unchanged, demonstrating the favorable operation stability and implying the desirable structural stability of the hybrid membranes.

3.2.4. Comparison of pervaporation performance of chitosan-based hybrid membranes

Chitosan, as a biopolymer, has been widely used in water-related membrane processes such as pervaporation dehydration, proton exchange membrane in fuel cell, as well as ultrafiltration for its high affinity towards water, adhesiveness, excellent film-forming and chemical resistance properties. Table 2 summarizes the pervaporation performance of chitosan-based hybrid membranes for the dehydration of ethanol reported in the literatures. It can be seen that the membrane in this work possessed an ultrathin active layer and the consequent high permeation flux, which was essential for the industrial application of membrane. Meanwhile, a favorable separation factor was also obtained.

4. Conclusion

Ultrathin, robust chitosan–titania hybrid membranes were obtained in a facile way by introducing DHPPA as a bioinspired multifunctional modifier to mediate the *in situ* sol–gel reaction of TiCl$_4$ within CS matrix. DHPPA played the following four roles: (1) retarding the sol–gel reaction of TiCl$_4$ to realize the uniform formation of inorganic particles with small size through metal–organic coordination interaction between DHPPA and titanium; (2) deterring the densification of hybrid membrane structure through steric hindrance effect together with suppressing the cross-linking reaction between polymer and inorganic precursor to prevent the decrease in membrane permeability; (3) forming hydrogen bonds and electrostatic attractions with CS polymer chains to improve the interfacial compatibility between polymeric continuous phase and inorganic dispersed phase; (4) enhancing the hydrophilicity of hybrid membrane *via* the plenty of carboxyl groups on DHPPA to facilitate the preferential sorption of water molecules on the membrane surface. As a result, the hybrid membranes exhibited higher swelling resistance, separation performance, as well as long-term operation stability. The hybrid membrane exhibited the optimal pervaporation performance with a permeation flux of 1403 g/(m^2 h) and a separation factor of 730 for 90 wt% ethanol aqueous solution at 350 K when the mass ratio of TiCl$_4$ to CS was 14 wt%.

Nomenclature

Symbols

A	membrane area (m^2)
E	apparent activation energy (kJ/mol)
F	mass fractions in feed solution (wt%)
J	permeation flux ($g/m^2\,h$)
l	membrane thickness (m)
P	mass fractions in permeate solution (wt%)
P/l	permeance (GPU)
Q	mass of permeate (g)
S_q	membrane surface roughness (nm)
t	time interval (h)
W	mass of membrane (g)
X	mass ratio of TiO_2 to CS (wt%)

Greek letters

α	separation factor
β	selectivity
γ	activity coefficient
θ	diffraction angle (deg)

Subscripts

D	dry membrane
E	ethanol
S	swollen membrane
W	water

Abbreviations

ACR	area change rate
MCR	mass change rate
PSI	pervaporation separation index

References

[1] J.H. Chen, J.Z. Zheng, Q.L. Liu, H.X. Guo, W. Weng, S.X. Li, Pervaporation dehydration of acetic acid using polyelectrolytes complex (PEC)/11-phosphotungstic acid hydrate (PW11) hybrid membrane (PEC/PW11), J. Membr. Sci. 429 (2010) 206–213.

[2] V.T. Magalad, G.S. Gokavi, M.N. Nadagouda, T.M. Aminabhavi, Pervaporation separation of water–ethanol mixtures using organic–inorganic nanocomposite membranes, J. Phys. Chem. C 115 (2011) 14731–14744.

[3] D. Yang, J. Li, Z.Y. Jiang, L.Y. Lu, X. Chen, Chitosan/TiO_2 nanocomposite pervaporation membranes for ethanol dehydration, Chem. Eng. Sci. 64 (2009) 3130–3137.

[4] Z.L. Xie, M. Hoang, T. Duong, D. Ng, B. Dao, S. Gray, Sol–gel derived poly(vinyl alcohol)/maleic acid/silica hybrid membrane for desalination by pervaporation, J. Membr. Sci. 383 (2011) 96–103.

[5] P.S. Rachipudi, A.A. Kittur, S.K. Choudhari, J.G. Varghese, M.Y. Karidurgaanavar, Development of polyelectrolyte complexes of chitosan and phosphotungstic acid as pervaporation membranes for dehydration of isopropanol, Eur. Polym. J. 45 (2009) 3116–3126.

[6] P.S. Rachipudi, A.A. Kittur, A.M. Sajjan, M.Y. Karidurgaanavar, Synthesis and characterization of hybrid membranes using chitosan and 2-(3,4-epoxycyclohexyl) ethyltrimethoxysilane for pervaporation dehydration of isopropanol, J. Membr. Sci. 441 (2013) 83–92.

[7] Y. Dai, J.R. Johnson, O. Karvan, D.S. Sholl, W.J. Koros, Ultem((R))/ZIF-8 mixed matrix hollow fiber membranes for CO_2/N_2 separations, J. Membr. Sci. 401 (2012) 76–82.

[8] T.T. Moore, R. Mahajan, D.Q. Vu, W.J. Koros, Hybrid membrane materials comprising organic polymers with rigid dispersed phases, AIChE J. 50 (2004) 311–321.

[9] T. Suzuki, Y. Yamada, Effect of thermal treatment on gas transport properties of hyperbranched polyimide–silica hybrid membranes, J. Membr. Sci. 417 (2012) 193–200.

[10] M. Amjadi, S. Rowshanzamir, S.J. Peighambardoust, S. Sedghi, Preparation, characterization and cell performance of durable nafion/SiO_2 hybrid membrane for high-temperature polymeric fuel cells, J. Power Sources 210 (2012) 350–357.

[11] Y.J. Yoon, T.H. Kim, D.M. Yu, Y.T. Hong, Sulfonated poly(arylene ether sulfone)/disulfonated silsesquioxane hybrid proton conductors for proton exchange membrane fuel cell application, Int. J. Hydrogen Energy 37 (2012) 18981–18988.

[12] Y.N. Zhao, Z.Y. Jiang, D.S. Lin, A.J. Dong, Z. Li, H. Wu, Enhanced proton conductivity of the proton exchange membranes by the phosphorylated silica submicropheres, J. Power Sources 224 (2013) 28–36.

[13] M.Y. Karidurgaanavar, S.S. Kulkarni, A.A. Kittur, Pervaporation separation of water–acetic acid mixtures through poly(vinyl alcohol)-silicone based hybrid membranes, J. Membr. Sci. 246 (2005) 83–93.

[14] S.S. Kulkarni, A.A. Kittur, M.I. Aralaguppi, M.Y. Karidurgaanavar, Synthesis and characterization of hybrid membranes using poly(vinyl alcohol) and tetraethylorthosilicate for the pervaporation separation of water–isopropanol mixtures, J. Appl. Polym. Sci. 94 (2004) 1304–1315.

[15] T. Uragami, T. Katayama, T. Miyata, H. Tamura, T. Shiraiwa, A. Higuchi, Dehydration of an ethanol/water azeotrope by novel organic–inorganic hybrid membranes based on quaternized chitosan and tetraethoxysilane, Biomacromolecules 5 (2004) 1567–1574.

[16] Q.G. Zhang, Q.L. Liu, J. Lin, J.H. Chen, A.M. Zhu, Analyzing solubility and diffusion of solvents in novel hybrid materials of poly(vinyl alcohol)/γ-aminopropyltriethoxysilane by inverse gas chromatography, J. Mater. Chem. 17 (2007) 4889–4895.

[17] J. Mosa, A. Duran, M. Aparicio, Epoxy-polystyrene-silica sol–gel membranes with high proton conductivity by combination of sulfonation and tungstophosphoric acid doping, J. Membr. Sci. 361 (2010) 135–142.

[18] N. Wang, C.M. Wu, Y.H. Wu, T.W. Xu, Hybrid anion exchange hollow fiber membranes through sol–gel process of different organic silanes within BPPO matrix, J. Membr. Sci. 363 (2010) 128–139.

[19] Q.G. Zhang, Q.L. Liu, A.M. Zhu, Y. Xiong, X.H. Zhang, Characterization and permeation performance of novel organic–inorganic hybrid membranes of poly(vinyl alcohol)/1,2-bis(triethoxysilyl)ethane, J. Phys. Chem. B 112 (2008) 16559–16565.

[20] J. Zhu, G. Zhang, K. Shao, C.J. Zhao, H.T. Li, Y. Zhang, M.M. Han, H.D. Lin, M. Li, H. Na, Hybrid proton conducting membranes based on sulfonated cross-linked polysiloxane network for direct methanol fuel cell, J. Power Sources 196 (2011) 5803–5810.

[21] F.A. Al-Sagheer, S. Merchant, Visco-elastic properties of chitosan–titania nanocomposites, Carbohydr. Polym. 85 (2011) 356–362.

[22] R.L. Guo, C.L. Hu, F.S. Pan, H. Wu, Z.Y. Jiang, PVA–GPTMS/TEOS hybrid pervaporation membrane for dehydration of ethylene glycol aqueous solution, J. Membr. Sci. 281 (2006) 454–462.

[23] Y. Chen, R. Wang, J.A. Zhou, H.J. Fan, B. Shi, Membrane formation temperature-dependent gas transport through thermo-sensitive polyurethane containing in situ-generated TiO_2 nanoparticles, Polymer 52 (2011) 1856–1867.

[24] F.B. Peng, L.Y. Lu, H.L. Sun, Y.Q. Wang, H. Wu, Z.Y. Jiang, Correlations between free volume characteristics and pervaporation permeability of novel PVA–GPTMS hybrid membranes, J. Membr. Sci. 275 (2006) 97–104.

[25] F.S. Pan, Q.L. Cheng, H.P. Jia, Z.Y. Jiang, Facile approach to polymer–inorganic nanocomposite membrane through a biomineralization-inspired process, J. Membr. Sci. 357 (2010) 171–177.

[26] M.L. DiVona, Z. Ahmed, S. Bellitto, A. Lenci, E. Traversa, S. Licoccia, SPEEK–TiO_2 nanocomposite hybrid proton conductive membrane via in situ mixed sol–gel process, J. Membr. Sci. 296 (2007) 156–161.

[27] J.J. Wilker, Marine bioinorganic materials: mussels pumping iron, Curr. Opin. Chem. Biol. 14 (2010) 276–283.

[28] J.J. Wilker, The iron-fortified adhesive system of marine mussels, Angew. Chem. Int. Ed. 49 (2010) 8076–8078.

[29] W.P. Liu, B. Li, R.J. Cao, Z.Y. Jiang, S.N. Yu, G.H. Liu, H. Wu, Enhanced pervaporation performance of poly (dimethyl siloxane) membrane by incorporating titania microspheres with high silver ion loading, J. Membr. Sci. 378 (2011) 382–392.

[30] Y.F. Li, S.F. Wang, H. Wu, J.T. Wang, Z.Y. Jiang, Bioadhesion-inspired polymer–inorganic nanohybrid membranes with enhanced CO_2 capture properties, J. Mater. Chem. 22 (2012) 19617–19620.

[31] H. Lee, N.F. Scherer, P.B. Messersmith, Single-molecule mechanics of mussel adhesion, Proc. Natl. Acad. Sci. 103 (2006) 12999–13003.

[32] H. Lee, S.M. Dellatore, W.M. Miller, P.B. Messersmith, Mussel-inspired surface chemistry for multifunctional coatings, Science 318 (2007) 426–430.

[33] J. Sedo, J. Saiz-Poseu, F. Busque, D. Ruiz-Molina, Catechol-based biomimetic functional materials, Adv. Mater. 25 (2013) 653–701.

[34] Q. Ye, F. Zhou, W.M. Liu, Bioinspired catecholic chemistry for surface modification, Chem. Soc. Rev. 40 (2011) 4244–4258.

[35] J.L. Dalsin, L.J. Lin, S. Tosatti, J. Voros, M. Textor, P.B. Messersmith, Protein resistance of titanium oxide surfaces modified by biologically inspired mPEG-DOPA, Langmuir 21 (2005) 640–646.

[36] B.P. Tripathi, M. Kumar, A. Saxena, V.K. Shahi, Bifunctionalized organic–inorganic charged nanocomposite membrane for pervaporation dehydration of ethanol, J. Colloid Interface Sci. 346 (2010) 54–60.

[37] G. Kim, L.Y. Hong, J. Jung, D.P. Kim, H. Kim, I.J. Kim, J.R. Kim, M. Ree, The biocompatability of mesoporous inorganic–organic hybrid resin films with ionic and hydrophilic characteristics, Biomaterials 31 (2010) 2517–2525.

[38] T. Uragami, S. Yanagisawa, T. Miyata, Water/ethanol selectivity of new organic–inorganic hybrid membranes fabricated from poly(vinyl alcohol) and an oligosilane, Macromol. Chem. Phys. 208 (2007) 756–764.

[39] J.T. Wang, S. Jiang, H. Zhang, W.J. Lv, X.L. Yang, Z.Y. Jiang, Enhancing proton conduction and methanol barrier performance of sulfonated poly(ether ether ketone) membrane by incorporated polymer carboxylic acid spheres, J. Power Sources 364 (2010) 253–262.

[40] J.H. Chen, Q.L. Liu, X.H. Zhang, Q.G. Zhang, Pervaporation and characterization of chitosan membranes cross-linked by 3-aminopropyltriethoxysilane, J. Membr. Sci. 292 (2007) 125–132.

[41] J. Ma, M.H. Zhang, L.Y. Lu, X. Yin, J. Chen, Z.Y. Jiang, Intensifying esterification reaction between lactic acid and ethanol by pervaporation dehydration using chitosan–TEOS hybrid membranes, Chem. Eng. J. 155 (2009) 800–809.

[42] H.L. Sun, L.Y. Lu, X. Chen, Z.Y. Jiang, Pervaporation dehydration of aqueous ethanol solution using H-ZSM-5 filled chitosan membranes, Sep. Purif. Technol. 58 (2008) 429–436.

[43] S. Qiu, L.G. Wu, G.Z. Shi, L. Zhang, H.L. Chen, C.J. Gao, Preparation and pervaporation property of chitosan membrane with functionalized multi-walled carbon nanotubes, Ind. Eng. Chem. Res. 49 (2010) 11667–11675.

[44] X. Chen, H. Yuan, Z.Y. Gu, Z.Z. Shao, Preparation and characterization of HY zeolite-filled chitosan membranes for pervaporation separation, J. Appl. Polym. Sci. 79 (2001) 1144–1149.

[45] D. Xu, L.S. Loo, K. Wang, Pervaporation performance of novel chitosan–POSS hybrid membranes: effects of POSS and operating conditions, J. Polym. Sci., Part B: Polym. Phys. 48 (2010) 2185–2192.

[46] Y.L. Liu, C.Y. Hsu, Y.H. Su, J.Y. Lai, Chitosan–silica complex membranes from sulfonic acid functionalized silica nanoparticles for pervaporation dehydration of ethanol–water solutions, Biomacromolecules 6 (2005) 368–373.

[47] H.L. Sun, L.Y. Lu, X. Chen, Z.Y. Jiang, Surface-modified zeolite-filled chitosan membranes for pervaporation dehydration of ethanol, Appl. Surf. Sci. 254 (2008) 5367–5374.